

HI observations of low surface brightness galaxies: Probing low-density galaxies

W.J.G. de Blok,¹ S.S. McGaugh^{2*} and J.M. van der Hulst¹

¹*Kapteyn Astronomical Institute, P.O. Box 800, 9700 AV Groningen, The Netherlands*

²*Institute of Astronomy, University of Cambridge, Madingley Road, Cambridge CB3 0HA, UK*

received: ; accepted:

ABSTRACT

We present Very Large Array (VLA) and Westerbork Synthesis Radio Telescope (WSRT) 21-cm HI observations of 19 late-type low surface brightness (LSB) galaxies. Our main findings are that these galaxies, as well as having low surface brightnesses, have low HI surface densities, about a factor of ~ 3 lower than in normal late-type galaxies. We show that LSB galaxies in some respects resemble the outer parts of late-type normal galaxies, but may be less evolved. LSB galaxies are more gas-rich than their high surface brightness counterparts. The rotation curves of LSB galaxies rise more slowly than those of HSB galaxies of the same luminosity, with amplitudes between 50 and 120 km s⁻¹, and are often still increasing at the outermost measured point. The shape of the rotation curves suggests that LSB galaxies have low matter surface densities. We use the average total mass surface density of a galaxy as a measure for the evolutionary state, and show that LSB galaxies are among the least compact, least evolved galaxies. We show that both M_{HI}/L_B and M_{dyn}/L_B depend strongly on central surface brightness, consistent with the surface brightness–mass-to-light ratio relation required by the Tully-Fisher relation. LSB galaxies are therefore slowly evolving galaxies, and may well be low surface density systems in all respects.

Key words: galaxies: evolution – galaxies: fundamental parameters – galaxies: structure – galaxies: spiral – galaxies: kinematics and dynamics – dark matter

1 INTRODUCTION

In recent years low surface brightness (LSB) galaxies have received an increasing amount of attention. With the advent of deep, large-field surveys many of these galaxies have been discovered, both in clusters and in the field (Schombert et al. 1988, 1992 [hereafter SBSM], Turner et al. 1993, Davies et al. 1994, Schwartzenberg et al. 1995, Sprayberry et al. 1995a).

The main property which distinguishes LSB galaxies from normal “classical” galaxies that define the Hubble sequence is their low surface brightness ($\mu_0(B) \gtrsim 23$) and not their size. LSB galaxies are not necessarily dwarfs. Many of them are disk galaxies that typically have scale lengths of several kpc, (McGaugh & Bothun 1994, de Blok et al. 1995 [hereafter BHB95]) i.e., in the same size range as typical high surface brightness (HSB) galaxies. The faintest LSB disk galaxies hitherto discovered have central surface brightnesses of ~ 26 mag arcsec⁻² (Turner et al. 1993; Irwin et al.

1990; Davies, Phillips & Disney 1988). This is almost two orders of magnitude fainter than those of the disk galaxies that obey Freeman’s Law (1970), which states that most disk galaxies have a central B -band surface brightness in the range 21.65 ± 0.30 mag arcsec⁻².

The existence of LSB galaxies with central surface brightnesses deviating many σ from the Freeman value indicates that this law is not a complete description of the central surface brightness distribution of disk galaxies. Attempts to construct the proper distribution from extant data (McGaugh, Bothun & Schombert 1995, McGaugh 1996) suggest that LSB galaxies are numerically common, though considerable uncertainty remains.

De Jong (1995, 1996) investigated the central surface brightness distribution of spiral galaxies for a range of Hubble types. He concluded, on the basis of a diameter-limited, statistically complete sample of 86 face-on spiral galaxies from the UGC (including a few LSB galaxies), that Freeman’s Law should be restated as that there is no preferred single value for the central surface brightness of disks in galaxies, but only an upper limit in surface brightness which galaxies can have (corresponding approximately to the Free-

* Present address: Department of Terrestrial Magnetism, Carnegie Institution of Washington, 5241 Broad Branch Road NW, Washington, DC 20015, USA

man value) (see also Allen & Shu, 1979). Towards later types the central surface brightness systematically decreases.

In general the range of properties exhibited by LSB galaxies is much larger than that of the classical Freeman galaxies. The sizes and luminosities of LSB galaxies range from the very small and faint dwarfs like GR8 (Hodge 1967), to the giant and luminous LSB galaxy Malin 1 (Impey & Bothun 1989, Sprayberry et al. 1995a). LSB galaxies *in general* are therefore likely to be not so much a single group, different from all other types of galaxies, but rather the dim counterparts of the known “classical” galaxies.

We have drawn our sample from the list of LSB galaxies by SBSM. The SBSM list was made by scanning by eye selected fields of the new POSS-II survey, and applying the UGC diameter selection criteria to the objects discovered. The increased depth of these new plates resulted in the discovery of many LSB galaxies that would have been in the UGC had it been compiled at present using the POSS-II plates. SBSM make no claims about completeness in their survey, but rather that “our purpose... is simply to increase our known sample of LSB galaxies and to offset the clear bias in apparent magnitude catalogs for the discovery of only HSB systems.” The present paper is written in this spirit.

With this in mind it is striking that LSB galaxy surveys that have concentrated on detecting field LSB galaxies (like e.g. SBSM) have in general found that the large majority of the galaxies ($\sim 85\%$ in the case of SBSM) in these surveys are late-type spirals. Ellipticals and early-type spiral galaxies form only a small minority. In our work we will therefore restrict ourselves to describing the properties of a subset of LSB galaxies: those of the late-type LSB disk galaxies. In the rest of the paper when we refer to LSB galaxies we will always implicitly mean this sub-group, unless noted otherwise. Not included are dwarf ellipticals and spheroids, like those found in the Local Group.

The group of late-type LSB galaxies is in many ways an extension of the Hubble-type sequence towards very late types. They continue (and are in many cases the most extreme representatives known of) the trends defined by the HSB galaxies along the Hubble sequence towards lower surface brightnesses. Such trends are increasingly bluer colours (BHB95, McGaugh & Bothun 1994 [hereafter MB94], Rönback 1993), decreasing oxygen abundances in the gas (McGaugh 1994, Rönback & Bergvall 1995), and decreasing HI surface densities (van der Hulst et al. 1993 [hereafter vdH93]). A detailed investigation of these late-type LSB disk galaxies will therefore provide an insight into systematic changes of properties of spiral galaxies along the Hubble sequence as an explicit function of surface brightness.

One particular example of the trends with surface brightness was presented in Zwaan et al (1995) (cf. Romanishin et al. 1982). It was shown that late-type LSB disk galaxies also lie on the Tully-Fisher relation (see also Sprayberry et al. 1995b), requiring a systematic and fine-tuned relation between the surface brightness of a galaxy and its overall mass-to-light ratio. In order to hope to understand this systematic relation, and perhaps to uncover other relations important to our understanding of galaxy properties and their history, resolved HI imaging, providing detailed rotation curves, is required.

We have obtained such HI imaging data for 19 LSB

galaxies with the VLA[†] and WSRT[‡] synthesis radio telescopes. In this paper we present the data and a global analysis. In forthcoming papers we will present a full decomposition of the rotation curves into disc and halo components, and, in combination with optical properties, discuss the processes that regulate the rate of evolution and star formation in these dim galaxies.

In Section 2 we discuss the sample selection. Section 3 contains technical details on the observations. In Section 4 we discuss the reduction of the data. In Section 5 the derivation of parameters from these data are given. In Section 6 we present the data in tabular and graphical form. Section 7 contains a discussion of the HI surface densities. In Section 8 the rotation curves are discussed. Section 9 is devoted to the mass-to-light ratios, and finally in Section 10 the main points of this paper are summarized.

2 SAMPLE SELECTION

We present 21-cm HI synthesis radio observations of a sample of 19 LSB galaxies, taken from the catalogues of LSB galaxies by SBSM. The SBSM catalogue is not dominated by small, faded dwarf galaxies. LSB galaxies occupy the full range of types as defined by the Hubble sequence, however with a strong preference towards later types.

The redshift distribution is similar to those of the UGC galaxies, with only small deviations at the low and high velocity tails, where the LSB survey picks up LSB dwarfs, and LSB giants respectively. The spatial distribution shows that LSB galaxies are good tracers of the large-scale structure on scales of > 2 Mpc (cf. Bothun et al. 1993; Mo, McGaugh & Bothun 1994). They do not fill the voids. The same applies to the distribution of HI masses: apart from a slightly smaller mean for the LSB galaxies, they are similar. The large fraction of LSB galaxies that has been detected in HI shows that these galaxies are just as likely to contain HI as their HSB counterparts of similar Hubble-type. We refer to SBSM for a complete discussion of the properties of the galaxies in their catalogue.

The typical LSB galaxy, as listed in SBSM, is therefore a late-type spiral galaxy in our local universe, with luminosity and HI mass not significantly different from late types already present in the UGC, but typically more extreme in surface brightness.

In order to select a number of representative galaxies from the SBSM catalogue, we have applied the following criteria.

(i) The galaxy should have been detected in HI. This necessarily limits the sample to the 171 galaxies that have been observed with Arecibo, but as explained in SBSM this does not bias the sample towards objects containing much HI, as the success rate of detections for these galaxies was at

[†] The Very Large Array of the National Radio Astronomy Observatory (NRAO) is operated by Associated Universities Inc. under contract with the National Science Foundation,

[‡] The Westerbork Synthesis Radio Telescope is operated by the Netherlands Foundation for Research in Astronomy with financial support from the Netherlands Organization for Scientific Research (NWO).

least 80% (and would have been higher if not for the limits imposed by the observable velocity range).

(ii) As the HI masses of galaxies in SBSM are strongly peaked around $10^9 M_\odot$ with a spread of 0.5 dex to both sides (cf. Fig. 5 in SBSM), we have selected only galaxies with HI masses in the range $8.5 < \log M_{\text{HI}} < 9.5$. This leaves 132 galaxies.

(iii) In order not to confuse true dwarfs with LSB disk galaxies we have furthermore restricted the sample to those galaxies with redshifts between 3000 and 8000 km s^{-1} , which SBSM define as “LSB disks” (cf. their Fig. 3). This leaves 95 galaxies.

(iv) From this sample of 95 galaxies, we selected 16 galaxies at random. This subsample represents in our opinion a typical cross-section of the larger sample of late-type LSB disk galaxies.

The sample is listed in Tables 1–3.

In order to compare the properties of these LSB galaxies with those of dwarf LSB galaxies and large LSB galaxies, we further supplemented the sample with examples of these two classes. The dwarf sample consists of 3 galaxies with HI masses smaller than $10^{8.5} M_\odot$ and redshifts smaller than 3000 km s^{-1} . These are F564-V3, F571-V2 and F583-1.

We used the sample of vdH93 to represent the large LSB galaxies. Although their HI masses are slightly larger, they set themselves apart from our main LSB sample mostly because of their larger optical scale lengths, and because of the fact that despite their low central surface brightness, they were included in the UGC catalogue.

Although our sample is not complete in a statistical sense, we have obtained a sample of galaxies which is representative of the late-type LSB disk galaxies found in the SBSM catalogue. We can use this sample to extend the range in surface brightness over which properties of disk galaxies are investigated towards lower surface brightnesses.

It should also be noted that, to the best of our knowledge, no HI-rotation curves of galaxies with central surface brightnesses fainter than 23.5 B -mag arcsec $^{-2}$ (the average surface brightness of our sample) have been published. There are only a handful of rotation curves available in the literature of LSB dwarfs ($\mu_0 \sim 23$), most of them DDO dwarfs (Carignan & Beaulieu 1988, Hoffman et al. 1996). This is surprising, given the fact that these galaxies are dark-matter dominated, providing ideal cases for the study of the dynamics and density distributions of the dark matter. The discussion on whether halos are isothermal or singular (see Flores & Primack 1994) depends very much on evidence provided by this same handful of rotation curves.

The sample presented here thus greatly extends the available data on galaxies in this still ill-charted LSB area of parameter space. This is currently the largest sample of LSB galaxies for which detailed optical, radio and abundance data are available (vdH93, McGaugh 1994, MB94, BHB95).

3 OBSERVATIONS

We observed 19 LSB galaxies in the 21-cm HI line. Observations of 10 galaxies were performed with the VLA in its 3-km (C) configuration using two IF systems, 27 antennas and 64 channels over a 3.125 MHz bandwidth. The spectra were

Hanning-smoothed on-line providing a velocity resolution of 20.6 km s^{-1} . Each galaxy was observed for 5 times 40 minutes interspersed with 5 minute observations of a phase calibrator. For bandpass calibration and the flux density scale we observed 3C286 with the same correlator settings as each galaxy. The observations were performed on 10, 16, 17 and 21 December 1990. Further details are given in Table 1.

The other 9 galaxies were observed with the WSRT. Each galaxy was observed for 12 hours with 38 baselines ranging from 72m to 2736m with 72m increments. Both IF systems were used and the correlator was set up to provide 64 channels over a bandwidth of 2.5 MHz. No on-line spectral smoothing was performed, so the highest possible velocity resolution is 9.9 km s^{-1} . Off-line Hanning smoothing reduces the velocity resolution to 16.5 km s^{-1} . Amplitude/phase and bandpass calibration was performed using observations of 3C147 and 3C286. The observations were done in June and September 1990 and May and August 1991.

4 REDUCTION

4.1 VLA data

The raw VLA databases of uv -plane visibilities were edited to remove interference and bad baselines. Observing conditions were generally quite good, and very little editing was actually necessary. The edited uv databases were transformed into data cubes with the AIPS routine HORUS.

Calibration was obtained from observations of standard VLA calibrators interspersed between segments of on-target observations, typically with several calibration observations per galaxy. The continuum was removed from the data cubes by subtracting the average of channels which contained no galaxy emission. These channels were carefully checked for signal from the galaxies, and a buffer space of several channels was left between the edges of the targets and the channels used to define the continuum. Deconvolution of sidelobes with CLEAN was found to be unnecessary, as the level of the sidelobes was in general far below the noise level.

The pixel size was set to 5×5 arcsec, providing good sampling of the almost round beam of 14×13 arcsec. The velocity resolution after Hanning smoothing was 20.6 km s^{-1} .

The r.m.s. noise in the individual, continuum-subtracted channelmaps after Hanning smoothing was 1.1 mJy/beam, except for one galaxy (F574-2) that was observed for a shorter period and had a r.m.s. noise in the channel maps of 1.6 mJy/beam. So in general the minimum detectable (3σ) column density in the full-resolution channel maps was $1.5 \cdot 10^{20}$ atoms cm^{-2} .

4.2 WSRT data

The raw uv data were calibrated using standard procedures (Bos et al. 1981) and Fourier-transformed to produce FITS data cubes. These were then reduced using the Groningen Image Processing System GIPSY (van der Hulst et al. 1992). The channel maps of all data cubes were inspected visually to determine which channel maps contained HI line-emission. The continuum was determined for each channel, in the same way as for the VLA data. A linear interpolation of the continuum was made over the central channels and

Table 1. List of Observations

Galaxy	R.A.	Dec	V_{central}	Instrument	Resolution	rms noise
(1)	(1950.0)	(1950.0)	(km s^{-1})	(5)	(arcsec)	(mJy/beam)
(1)	(2)	(3)	(4)	(5)	(6)	(7)
F563-V1	08 43 48.1	19 04 26	3931	VLA	13.2×14.1	1.0
F563-V2	08 50 14.8	18 37 34	4316	VLA	13.1×14.0	1.1
F567-2	10 15 11.4	21 18 47	5683	VLA	13.4×14.6	1.2
F568-1	10 23 22.8	22 40 58	6522	VLA	13.6×15.5	1.3
F568-3	10 24 14	22 28 51	5912	VLA	12.9×14.0	1.0
F568-V1	10 42 19.9	22 19 20	5796	VLA	13.3×13.9	1.2
F571-V1	11 23 41.2	19 06 24	5705	VLA	13.4×14.3	1.1
F574-2	12 44 19	22 04 34	6322	VLA	13.6×15.3	1.6
F577-V1	13 47 56.4	18 31 01	7777	VLA	13.3×14.7	1.2
F579-V1	14 30 38	22 58 59	6302	VLA	12.9×14.3	1.1
F561-1	08 06 35	22 42 25	4810	WSRT	13.0×33.0	1.7
F563-1	08 52 10	19 56 35	3495	WSRT	12.8×37.1	1.7
F564-V3	09 00 03	20 16 23	480	WSRT	12.6×36.1	1.5
F565-V2	09 34 47	21 59 46	3677	WSRT	12.7×37.2	1.5
F571-8	11 31 18	19 37 53	3720	WSRT	13.2×39.3	1.5
F571-V2	11 34 53	18 41 10	958	WSRT	12.8×39.7	1.7
F574-1	12 35 38	22 35 20	6888	WSRT	13.0×33.0	1.6
F583-1	15 55 17	20 48 21	2277	WSRT	13.0×35.0	1.6
F583-4	15 49 58	18 55 58	3621	WSRT	12.8×39.2	1.8

- (1) Name of the galaxy
(2) Right Ascension of pointing center (1950.0)
(3) Declination of pointing center (1950.0)
(4) Central velocity (km s^{-1})
(5) Instrument used to do observation
(6) Size of synthesized beam (arcsec)
(7) Root-mean-square noise (mJy beam^{-1})

the continuum value was subtracted. The channel maps at the edges of the passband were not used in making the interpolation, as these maps were unusable due to the high noise level caused by the decreasing gain at the edges of the passband. This usually meant that the fits to the central continuum values were constrained by approximately 15 to 20 channel maps.

The resulting continuum-subtracted data cubes were Hanning-smoothed, decreasing the effective velocity resolution from 9.9 to 16.5 km s^{-1} . The data cubes did not need to be CLEAN-ed, as the strength of the emission was too low to show the effects of the sidelobes. The r.m.s. noise in the channel maps (after Hanning smoothing) was 1.6 mJy/beam , corresponding to a minimum detectable column density (3σ) of $1 \cdot 10^{20}$ atoms cm^{-2} . Note that the better sensitivity of the WSRT data is caused by the longer integrations and the larger beam.

5 THE DATA

In the rest of this paper we will refer to the number of atoms cm^{-2} (or alternatively $M_{\odot} \text{pc}^{-2}$) as projected on the sky, i.e. *not corrected* for inclination, as “*column density*”, while the term “*surface density*” will be used for the number of atoms cm^{-2} ($M_{\odot} \text{pc}^{-2}$) *corrected* for inclination effects.

5.1 Total column density maps and velocity fields

In order to construct the total column density maps – showing the integrated HI emission – and the velocity fields, the data cubes were smoothed to approximately half of their original spatial resolution (i.e., to 40×40 arcsec for the WSRT data and to 25×25 arcsec for the VLA data). All pixels below 2σ as measured in the channel maps of the smoothed cubes were blanked and remaining spurious noise peaks were removed. The non-blanked areas were used as masks for the cubes at the original resolution, and only those pixels in the original cubes that corresponded with non-blank pixels were retained. For each spatial position in the cube the HI profile moments were determined to construct the total HI column density maps and velocity fields.

5.2 Ellipse parameters

In general the galaxies were too face-on and too small to make a good tilted-ring model fit to the velocity fields and determine a reliable value for the kinematical inclination. So in most cases the inclination was determined either from the column density map after correcting for the shape of the beam, or the optical images (MB94, BHB95), or both. A check was made to see whether the value thus found was consistent with tentative values derived from the velocity fields. The position angles of the major axes and the positions of the dynamical centers of the galaxies were determined by inspecting the sequence of channel maps. See Table 2 for further details. The kinematical position angle is well deter-

Table 2. Inclination and position angle

Name	type	i	P.A.
(1)	(2)	(3)	(4)
F561-1	1	24	55
F563-1	1,2,3	25	-19
F563-V1	2	60	-40
F563-V2	2	29 ^a	-32
F564-V3	1	30	156
F565-V2	1,2	60	-155
F567-2	2	20	119
F568-1	1,2,3	26	13
F568-3	1,2	40	169
F568-V1	1,2	40	-44
F571-8	1,2,3	90	165
F571-V1	1,2	35	45
F571-V2	2	45	-150
F574-1	1,2	65	100
F574-2	1,2	30	53
F577-V1	1,2	35	40
F579-V1	1,2	26	120
F583-1	1,2,3	63	-5
F583-4	1,2	55	115

(1) Name of the galaxy

(2) Type of inclination used for final value. ‘1’ denotes optical inclination, ‘2’ HI inclination, and ‘3’ kinematical inclination.

(3) The resulting best value for the inclination in degrees.

(4) The position angle in degrees of the approaching side of the major axis, measured from N through E.

Note:

^a Optical inclination is 39 degrees and well determined. It may however be affected by central barlike structure, and was not used.

mined, and usually accurate to within 5 degrees. Errors in the inclination are difficult to estimate, and actually depend on the value of the inclination itself, but we are confident that the values are accurate to at least within 5 degrees, in most cases even better.

5.3 Radial column density profiles and position-velocity diagrams

Radial column density profiles were produced by integrating the column density maps in elliptical annuli, with ellipse parameters as given in Table 2.

The position-velocity diagrams were constructed by making a slice of 15 arcsec width through the cubes along the major axis in the velocity direction.

5.4 Rotation curves

The rotation curves were derived from the position-velocity diagrams by measuring the velocities of the maxima of the HI emission along the major axis. Beam-smearing was taken into account in the inner parts of the galaxies, where the gradient in the rotation curve is largest. The effects are however negligible (less than a few percent). The rotation curves were each derived twice, independently by dB and McG, and subsequently compared. In all cases the curves agreed within the errors.

Fits to the rotation curves were made by using a spline

fit to the average of the symmetrized data in a plot of $|V - V_{\text{sys}}|$ vs $|r - r_0|$. The values of V_{sys} and r_0 were chosen to minimize asymmetries; usually each is approximately the half way point between the extremes of the respective variables. The systemic velocities determined in this way are in excellent agreement with the single dish values from SBSM (Fig. 1). The mean absolute difference is 4 km s^{-1} , which is less than half of one of our channel separations.

6 RESULTS

The data are presented in Fig. 2 and in Table 3. Following is a description of the various panels in Fig. 2, and the columns in Table 3.

6.1 Figures

(a) R-band image with HI overlay. The optical R -band images are shown in grayscale. For a full description of these images see BHB95, McGaugh et al. (1995) and Appendix A. The contour levels represent HI column densities of 1, 3, 5, 7... $\times 10^{20}$ atoms cm^{-2} .

The coordinate systems of the optical and radio data were aligned by determining the right ascensions, declinations and pixel coordinates of 8 field stars in each R -band image. The right ascensions and declinations of the field stars are taken from POSS plates. The formal errors in aligning the two coordinate systems were at most 0.3 arcsec.

(b) B-band images For further details see BHB95 and McGaugh et al. (1995). For galaxies F571-8, F574-1, F579-V1, F583-1 and F583-4 a B -band image was not available, and a R -band image was used instead (see Appendix A). Galaxy F571-V2 is not visible in the R -band image, due to the presence of a bright star. We have instead retrieved an image of this galaxy from the red digital Palomar Sky Survey which is presented here.

(c) HI column density maps and velocity fields The black contours and grayscales represent 1, 3, 5, 7... $\times 10^{20}$ HI atoms cm^{-2} . The beam shown in the lower right corner has size 13×14 arcsec for the VLA data, and on average 13×35 arcsec for the WSRT data. The bar in the lower left corner shows the linear scale at the distance of the galaxies, assuming $H_0 = 100 \text{ km s}^{-1} \text{ Mpc}^{-1}$.

The velocity field is shown in white contours superimposed on the column density map. The velocity values corresponding to the respective contours are given in the captions to Fig. 2.

(d) Position-velocity diagrams The contour levels are $-2, 2, 3, 4... \sigma$, where σ is the standard deviation in the velocity slice. One σ equals 1.7 mJy/beam for the VLA data and 2.5 mJy/beam for the WSRT data. The horizontal dashed line shows the systemic velocity as derived from our symmetrization of the rotation curve, while the vertical line shows the spatial position of the center of rotation, also derived from symmetrization.

(e) **Radial surface density profiles** Radial column density profiles were determined from averaging in elliptical annuli (“rings” in the plane of the galaxy). These were corrected for inclination. Shown are therefore the radial *surface density* profiles. The error bars indicate the uncertainties in the values, and their size is given by:

$$\sigma_{\text{tot}} = \sigma_{\text{ch}} \cdot \frac{4}{\sqrt{6}} \cdot \frac{\sqrt{N - 0.75}}{\sqrt{\text{beams}/\text{ring}}}$$

where N is the number of channels contributing to a pixel in the total column density map ($N \simeq 3$), and σ_{ch} is the r.m.s. noise in a single channel map.

The lower horizontal axis gives the linear distance in kpc, using the distances from Table 3; the upper horizontal axis shows the corresponding angular distance in arcseconds.

In the case of F571-8 we show both the *observed* (edge-on) column density distribution and the deduced face-on surface density distribution. As F571-8 is an edge-on galaxy, deriving the latter distribution is not straight-forward. We have made an attempt, shown in the inset in panel (e) of the F571-8 panels, by dividing the galaxy into concentric rings (as seen face-on), assuming that gas is everywhere present at the line of nodes, and by working our way from the outside in, subtracting the contributions of subsequent rings, taking into account the lines of sight through each particular ring. This assumes of course that the HI is optically thin everywhere.

(f) **Rotation curves** The rotation curve data shown here are corrected for inclination. The drawn line is the symmetrical approximation to the data. See Section 5.4 for more detailed information. The open dots always correspond to the receding side of the galaxy, while the filled dots correspond to the approaching side. Again the bottom axis shows the radius in kpc, while the top axis shows the angular distance in arcseconds. The arrow indicates one optical disk scale length.

6.2 Table

Following is a description of the contents of Table 3.

Column (1): The name of the galaxy (SBSM).

Column (2): Heliocentric systemic velocity V_{sys} , defined as the center velocity in km s^{-1} of the symmetrized rotation curves.

Column (3): Distance D in Mpc, as derived from the heliocentric systemic velocity, given in Column (2), after correction for Galactic rotation and a Virgocentric flow of 300 km s^{-1} (where necessary) and assuming $H_0 = 100 \text{ km s}^{-1} \text{ Mpc}^{-1}$.

Column (4): Logarithm of the total HI mass M_{HI} . The total HI-mass, given in M_{\odot} , is derived from the total flux using the formula

$$M_{\text{HI}}/M_{\odot} = 2.36 \cdot 10^5 D(\text{Mpc})^2 \int S(\text{Jy}) dV(\text{km s}^{-1})$$

The fluxes are in good agreement with the single dish fluxes from SBSM. Figure 3 compares the synthesis and single dish fluxes, and shows that the synthesis observations measure all the flux.

Column (5): Maximum rotation velocity V_{max} of the rotation curve, not corrected for inclination.

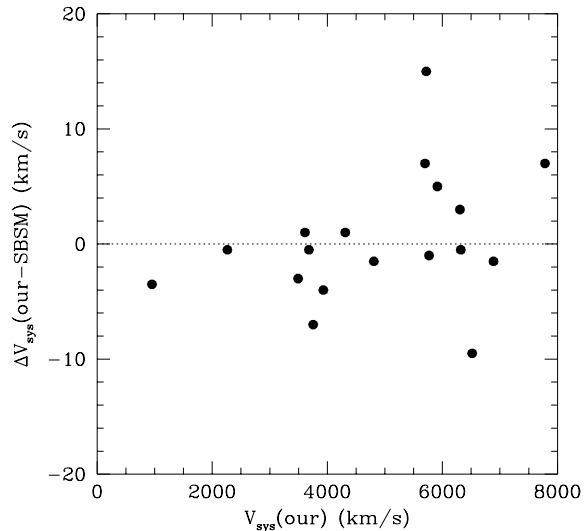


Figure 1. Difference between systemic velocities as determined from our rotation curves and the velocities obtained by SBSM using the Arecibo single dish telescope.

Column (6): Outer rotation velocity V_{out} . This is the rotation velocity in km s^{-1} as measured at the outermost point of the rotation curve. This value is not corrected for inclination.

Column (7): Outermost radius R_{out} . This is the radius in arcsec where V_{out} is measured and is the maximum radius at which the rotation curve could be measured.

Column (8): Logarithm of the dynamical mass M_{dyn} encompassed at the last measured point. This dynamical mass was derived using the formula

$$M_{\text{dyn}} = \frac{V_{\text{out}}^2 R_{\text{out}}}{G \sin^2 i},$$

where R_{out} is expressed in linear units.

Column (9): Ratio $M_{\text{HI}}/M_{\text{dyn}}$, the ratio of HI mass and dynamical mass.

Column (10): HI radius R_{HI} . The radius R_{HI} is defined as the radius where the azimuthally averaged *surface* density falls below $1 M_{\odot} \text{ pc}^{-2}$. Note that this radius is measured in the inclination corrected radial *surface* density profile. As F571-8 is an edge-on galaxy, the value given here for that galaxy should not be directly compared with the values for the other galaxies.

Column (11): Radius in arcseconds of the 25 B -mag arcsec $^{-2}$ isophote R_{25} .

Column (12): Adopted inclination (see Table 2).

Column (13): Peak smoothed column density σ_{smo} . In order to better compare the peak surface densities as measured with the VLA and the WSRT, the VLA data was smoothed to 35×13 arcseconds resolution (which is the WSRT resolution) and the resulting peak column densities are given.

Column (14): Peak column density σ_{peak} . This is the peak column density in each galaxy expressed in $M_{\odot} \text{ pc}^{-2}$.

Table 3. Properties of the sample of LSB galaxies.

Name	V_{sys}	D	M_{HI}	V_{max}	V_{out}	R_{out}	M_{dyn}	$\frac{M_{\text{HI}}}{M_{dyn}}$	R_{HI}	R_{25}	i
(1)	(2)	(3)	(4)	(5)	(6)	(7)	(8)	(9)	(10)	(11)	(12)
F561-1	4809	47	8.91	21	21	33	9.66	0.177	33.2	21	24
F563-1	3492	34	9.19	47	47	81	10.58	0.041	99.0	23	25
F563-V1	3932	38	8.48	26	24	30	9.00	0.283	26.1	13	60
F563-V2	4312	46	9.11	54	54	31	10.30	0.064	39.3	23	29
F564-V3	476	6	7.11	*	*	*	*	*	37.8	11	30
F565-V2	3681	36	8.53	44	44	36	9.58	0.089	29.1	10	60
F567-2	5698	56	9.09	22	22	31	9.91	0.152	39.0	9	20
F568-1	6517	64	9.35	52	51	36	10.55	0.064	37.1	18	26
F568-3	5913	58	9.20	77	77	44	10.62	0.038	40.4	21	40
F568-V1	5768	60	9.14	80	80	49	10.71	0.027	36.8	16	40
F571-8	3754	36	8.91	133	133	67	10.68	0.017	(95)	33	90
F571-V1	5719	59	8.82	42	42	38	10.13	0.049	26.0	10	35
F571-V2	955	12	7.81	32	32	47	9.12	0.049	41.1	*	45
F574-1	6889	72	9.29	91	91	33	10.43	0.072	34.5	38	65
F574-2	6319	66	8.97	20	20	25	9.50	0.293	29.2	9	30
F577-V1	7783	80	9.15	17	16	23	9.20	0.891	28.4	17	35
F579-V1	6305	64	9.06	52	44	42	10.49	0.037	48.3	27	26
F583-1	2264	24	8.99	79	79	94	10.27	0.052	91.2	21	63
F583-4	3612	37	8.49	55	55	42	9.90	0.0389	30.2	27	55

Name	σ_{smo}	σ_{peak}	σ_{aver}	$\mu_B(0)$	α_B	$\frac{R_{\text{HI}}}{R_{25}}$	M_B	L_B	$\frac{M_{\text{HI}}}{L_B}$	$\frac{M_{dyn}}{L_B}$	slope
	(13)	(14)	(15)	(16)	(17)	(18)	(19)	(20)	(21)	(22)	(23)
F561-1	5.88	5.88	4.80	23.28	11.9	1.58	-17.2	9.08	0.68	3.9	0.144
F563-1	6.28	6.28	4.94	23.63	19.7	4.30	-16.7	8.88	2.06	50.1	0.186
F563-V1	6.45	8.91	6.88	24.30	9.7	2.01	-15.7	8.49	0.91	3.2	0.209
F563-V2	8.89	14.46	7.92	22.10	7.0	1.71	-17.6	9.23	0.76	11.8	0.204
F564-V3	4.82	4.82	2.56	24.05	11.2	3.60	-12.1	7.04	1.18	*	*
F565-V2	7.13	7.13	6.16	24.73	11.5	2.91	-14.8	8.11	2.62	29.4	0.607
F567-2	4.83	7.6	4.23	24.42	15.8	4.33	-16.8	8.90	1.56	10.3	0.251
F568-1	8.63	13.39	8.93	23.77	12.9	2.06	-17.5	9.19	1.45	22.8	0.093
F568-3	6.79	8.67	6.09	23.08	10.8	1.92	-17.7	9.27	0.86	22.5	0.324
F568-V1	7.04	10.32	5.24	23.30	8.2	2.30	-17.3	9.10	1.11	41.1	0.293
F571-8	21.35	21.35	20.41	22.12	16.0	2.87	-17.0	8.99	0.83	49.0	0.575
F571-V1	4.85	7.21	6.05	24.00	8.4	2.61	-16.4	8.76	1.14	23.4	0.345
F571-V2	8.09	8.09	5.05	*	*	*	*	*	*	*	0.429
F574-1	10.33	10.33	6.81	23.31	10.0	0.91	-17.8	9.32	0.93	12.9	0.714
F574-2	4.32	7.84	4.36	24.35	14.0	3.24	-17.0	9.00	0.93	3.2	0.665
F577-V1	5.83	8.81	5.00	23.95	11.1	1.67	-17.6	9.23	0.83	0.9	-0.085
F579-V1	4.53	7.65	3.99	22.83	10.0	1.79	-18.2	9.48	0.38	10.2	-0.015
F583-1	14.18	14.18	10.12	24.03	10.2	4.34	-15.9	8.55	2.74	52.3	0.368
F583-4	3.99	3.99	3.14	23.76	11.3	1.11	-16.3	8.72	0.59	15.1	0.747

- (1) Name of galaxy
 (2) Systemic velocity (km s^{-1})
 (3) Distance (Mpc)
 (4) Logarithm of HI mass (M_{\odot})
 (5) Max. uncorrected rotation velocity (km s^{-1})
 (6) Outer uncorrected rotation velocity (km s^{-1})
 (7) Radius outermost point rotation curve (arcsec)
 (8) Logarithm of dynamical mass (M_{\odot})
 (9) Ratio HI mass to dynamical mass
 (10) Radius 1 $M_{\odot} \text{ pc}^{-2}$ HI level (arcsec)
 (11) Radius 25 B -mag arcsec^{-2} isophote (arcsec)
 (12) Inclination (see Table 2)
- (13) Smoothed peak column density ($M_{\odot} \text{ pc}^{-2}$)
 (14) Actual peak column density ($M_{\odot} \text{ pc}^{-2}$)
 (15) Radial peak column density ($M_{\odot} \text{ pc}^{-2}$)
 (16) Central surface brightness disc (B -mag arcsec^{-2})
 (17) Optical scale length in B (arcseconds)
 (18) Ratio HI diameter and optical diameter
 (19) Absolute magnitude (B -mag)
 (20) Logarithm of luminosity in B (L_B^B)
 (21) HI mass to light ratio (M_{\odot}/L_B^B)
 (22) Dynamical mass to light ratio (M_{\odot}/L_B^B)
 (23) Slope of rotation curve

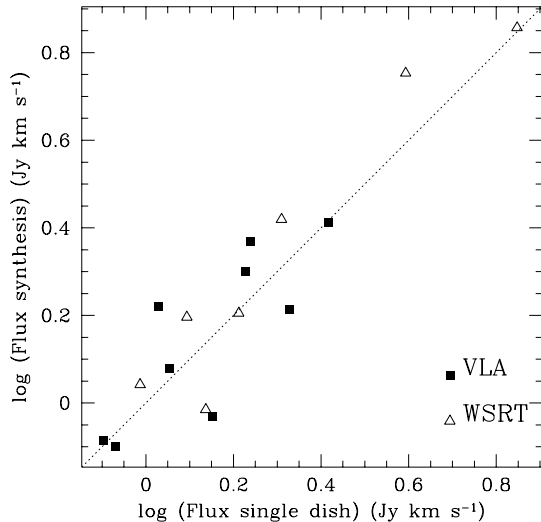


Figure 3. Total flux of the HI emission as measured with the VLA and WSRT plotted against the flux measured with the Arecibo single dish telescope (SBSM). The dotted line is the line of equality.

Column (15): Peak radial averaged surface density σ_{aver} . This is the maximum of the radial profile in $M_{\odot} \text{pc}^{-2}$.

The following columns contain a number of parameters related to the optical properties of the galaxies. These are taken from MB94 or BHB95. The optical properties of F571-8, F574-1, F579-V1 and F583-4 are converted from R -band measurements. See Appendix A for a description.

Column (16): Central B -band surface brightness μ_0 of the exponential disc, expressed in mag arcsec^{-2} , corrected for inclination, but not for internal extinction.

Column (17): Optical exponential B -band scale length α in arcseconds.

Column (18): Ratio of the optical and the HI diameter R_{HI}/R_{25} .

Column (19): Absolute magnitude M_{abs} , using D as given in column (3).

Column (20): Total intrinsic luminosity L_B , expressed in L_{\odot} , derived from M_{abs} , assuming $M_{\odot,B} = 5.48$.

Column (21): Total hydrogen-mass to total light ratio M_{HI}/L_B , expressed in solar units.

Column (22): Total dynamical-mass to light ratio M_{dyn}/L_B in solar units.

Column (23): The outer slope of the rotation curve. See Section 8.1 for more details.

7 SURFACE DENSITIES

In this section we will compare our data with samples of HSB galaxies, and show that indeed LSB galaxies have systematically lower HI surface densities than HSB galaxies.

It is a well-known fact that properties of galaxies change along the Hubble sequence. One of these properties is the average surface density of the atomic hydrogen σ_{HI} . This

changes from a value of $\sim 1 M_{\odot} \text{pc}^{-2}$ for Sa galaxies to a value of $\sim 8 M_{\odot} \text{pc}^{-2}$ for late-type galaxies (Roberts & Haynes 1994). Observations by vdH93 did show that LSB galaxies do not follow this trend. The σ_{HI} of the LSB galaxies investigated in vdH93 is a factor of two lower than in HSB galaxies of comparable morphological type. Note that this does not mean that LSB galaxies are therefore also more gas-poor. On the contrary, the gas fraction is significantly higher than in HSB galaxies, as we will show in Section 9.

Here we will compare the average and local HI properties of HSB and LSB galaxies, and discuss the relation between surface brightness and surface density – the relation between stars formed, and material from which to form stars – which can tell us something about the evolution of LSB galaxies.

7.1 Average surface densities

In order to make a comparison between average HI surface densities of HSB and LSB galaxies we need a sample of undisturbed HSB galaxies. Cayatte et al. (1994) have composed such a sample. Their field galaxy comparison sample consists of 84 galaxies with data taken from Warmels (1988) and Broeils (1992). Galaxies with large scale disturbances either in radio or optical were excluded and only galaxies with Hubble type between S0 and Sdm and inclinations smaller than 80 degrees were chosen. This sample therefore constitutes a sample of undisturbed HSB normal Hubble sequence galaxies, with central surface brightnesses typically between 21 and 23 B -mag arcsec^{-2} , i.e. from the Freeman value down to values approaching those of the LSB sample. One should therefore not think of the HSB sample as a collection of Freeman galaxies. The typical surface brightness of a typical galaxy from the HSB sample is, however, some two magnitudes brighter than that of a typical galaxy from the LSB sample. The distinction between HSB and LSB galaxies is merely a convenient way to describe two subsets of the continuum of galaxies.

Cayatte et al. defined the average HI surface density σ_{HI} as the average surface density of the HI within half of the optical radius R_{25} . The distribution of average surface density with Hubble-type is shown in Fig. 4. The surface density increases from Sa to Sc, and then slightly declines towards Sm galaxies.

We have computed σ_{HI} for our LSB galaxies in a similar manner. The average surface density of LSB galaxies is also shown in Fig. 4. It is clear that late-type LSB galaxies in our sample have average HI surface densities which are on average a factor of 3 lower than those of HSB galaxies of comparable type.

If we regard LSB galaxies as the continuation of the Hubble sequence towards extremely late types, LSB galaxies would simply continue the trend of decreasing HI surface density seen in Fig. 4 from type Sc onwards.

The Hubble sequence is then a sequence of increasing atomic gas surface density from S0 to Sc, and decreasing surface density for the later types. A very interesting question is whether this decreasing trend continues towards progressively lower surface brightnesses. At a certain point the gas will be diluted enough for the intergalactic radiation field to completely ionize it. Calculations by e.g. Dalcanton, Spergel & Summers (1995) and Maloney (1993) show that this can

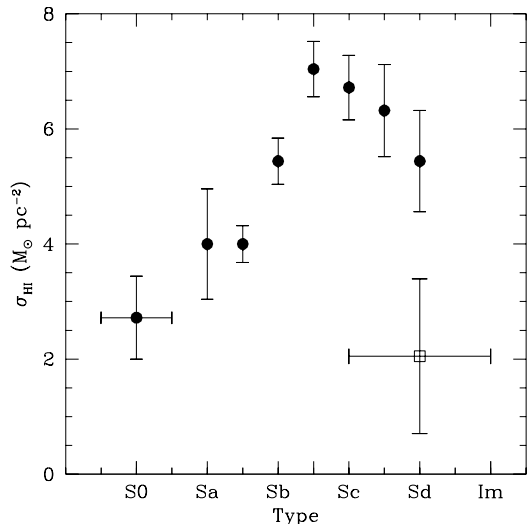


Figure 4. LSB galaxies and their place in the Hubble-type – average HI surface density diagram. The average surface density is defined as the average surface density of the HI within half of the optical radius R_{25} . Filled circles are HSB galaxies from the sample of Cayatte et al. (1994). Vertical errorbars are the 1σ errors in the mean. The open square represents our sample of LSB galaxies. Horizontal errorbars denote the range in type in our sample, vertical errorbars are 1σ deviations from the mean.

already happen at HI-surface densities of a few times 10^{19} cm^{-2} . This would imply a minimum surface brightness a galaxy can have below which it will become completely ionized (Quinn, Katz & Efsthathiou 1995).

One could furthermore speculate that the low gas surface densities measured for types earlier than Sc are caused by the rapid gas consumption due to the high star formation rate in these galaxies (see e.g. Guiderdoni & Rocca-Volmerange 1987). In this picture the peak in Fig. 4 would then shift towards later types as time (and gas consumption, and other evolutionary processes) progresses.

7.1.1 Isophotal ratios

As was already remarked in MB94 and BHB95, one should be cautious in using isophotal quantities for a direct comparison between HSB and LSB galaxies. There is therefore also a danger in using optical radii to determine average quantities, like the average surface density within half an optical radius, as was done above. Quantities like R_{25} become less representative as one goes towards lower surface brightnesses, and may lose their meaning altogether (in this specific case, if the galaxy has a central surface brightness fainter than $25 \text{ mag arcsec}^{-2}$).

This of course also applies to ratios of such quantities, like the ratio R_{HI}/R_{25} (see column (18) of Table 3). This is not a very useful quantity for a quantitative comparison of HSB and LSB galaxies. The low surface brightness of LSB galaxies ensures that the R_{25} will substantially underestimate the real optical size of the galaxy, and artificially

raises the value of the ratio. It is obvious that quantities like σ_{HI} , as defined above, will then also be affected.

In this case R_{25} will, however, always decrease faster with decreasing central surface brightness than any of the HI parameters. This alone will already artificially raise the computed average surface density, so that the discrepancy between HSB and LSB galaxies might in reality be larger than suggested by Fig. 4. We will come back to this in the next section.

R_{HI} can also suffer from the same problem as R_{25} : as the HI surface density in LSB galaxies is much lower than in HSB galaxies, it will underestimate the size of the HI disc. This is apparent if one compares the distribution of values of R_{HI} of HSB galaxies with that of LSB galaxies. These distributions are comparable, which one naively would not expect as LSB galaxies are more extended. However, as the surface density is lower in LSB galaxies, this simply means that, for a HSB and a LSB galaxy with the same total HI-mass and R_{HI} , there is more HI present outside R_{HI} in the LSB galaxy. So comparing galaxies with identical HI mass *inside* R_{HI} is not correct, as one then compares a more massive LSB galaxy with a lower mass HSB galaxy.

This once again shows that isophote and iso-density effects should always be taken into account when comparing galaxies of different surface brightnesses and surface densities.

7.2 Radial density profiles

Ideally, we would like to see if LSB galaxies have consistently lower surface densities at all radii. For that we need to compare the radial HI profiles of LSB galaxies with those of a sample of “classical” field galaxies.

For this we again use the sample of Cayatte et al. (1994) as they have calculated the average HI surface density profiles of galaxies of different Hubble-types.

Unfortunately they give the average radial HI profile for each Hubble-type as a function of R/R_{25} . As isophotal effects are more severe in the optical than in HI, we have re-normalized the radial profiles of the HSB galaxies to R/R_{HI} , using the mean values of R_{25}/R_{HI} as given in Cayatte et al. (1994). We have made a correction for the different definition they use for R_{HI} .

These profiles are presented in Fig. 5. Note that the trend shown in Fig. 4 of surface density with Hubble-type is also apparent in the local surface densities. Local surface density values increase from early types to Sc/Sd and then decrease again. The average radial surface density profile of our sample of LSB galaxies is shown as the heavy line in Fig. 5.

It is clear from Fig. 5 that the HI surface density of an average late-type LSB galaxy is lower than or comparable to the profiles of early-type HSB galaxies, and again a factor of 3 lower than those of late-type galaxies. This of course requires a LSB galaxies of a given HI-mass to be more extended than HSB galaxies of the same HI mass.

7.3 Surface brightness and surface density

The result that LSB galaxies, apart from having lower surface brightnesses, also have lower HI surface densities shows

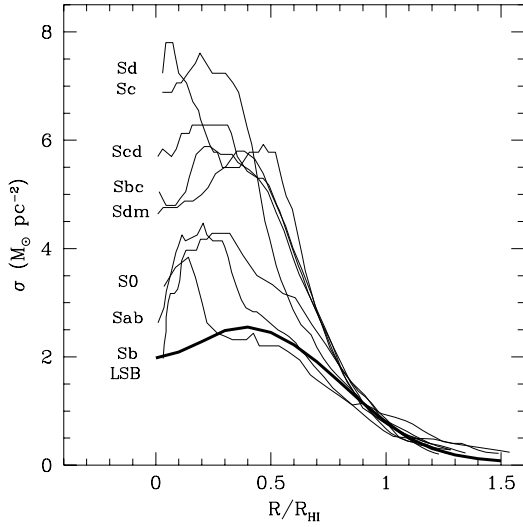


Figure 5. The average radial distribution of HI for HSB galaxies of different Hubble-types (light lines) (Cayette et al. 1994) and LSB galaxies (heavy line). Radii have been normalized to R_{HI} (see text).

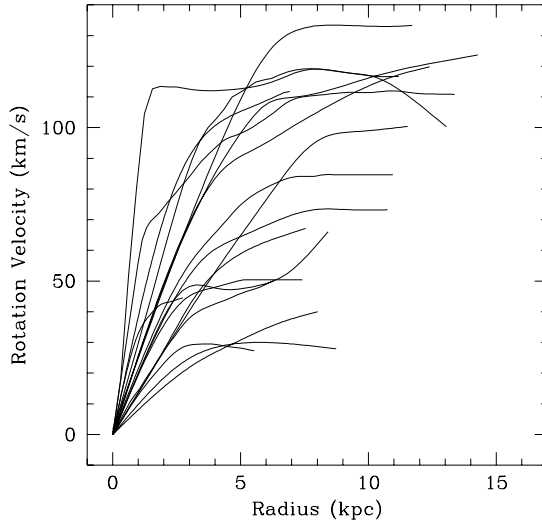


Figure 7. Inclination corrected rotation curves of our sample of LSB galaxies.

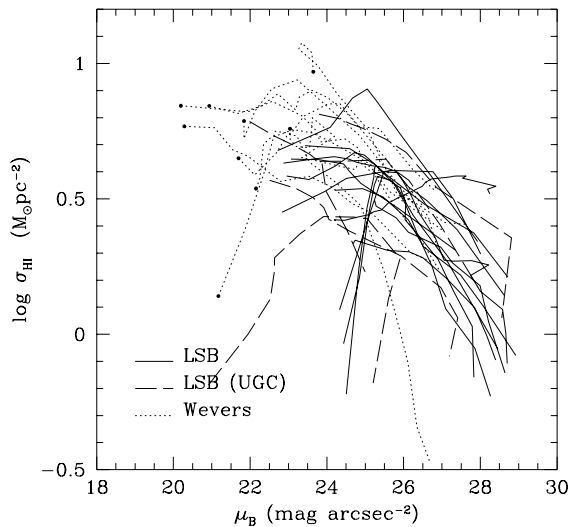


Figure 6. The relation between local optical surface brightness and local HI surface density. The HSB galaxies from Wevers et al. (1986) are represented by dotted lines, LSB galaxies from our sample by the heavy, drawn lines, and the LSB galaxies from vdH93 by dashed lines.

that there is a relation between the luminosity surface density and the gas surface density. We have tested this idea by taking the photometry and the HI data from the sample of Wevers et al. (1986), where we have converted his J -band photometry to B -band photometry using the conversion formulae given by him. The maximum error in the conversion formulae is ± 0.10 mag. However, the uncertainties in the surface brightness are dominated by the uncertainties in the flux-calibration, so the surface brightnesses of the Wevers galaxies are uncertain by ± 0.20 mag arcsec $^{-2}$. As we will see this is of sufficient quality to make a comparison with our photometry.

Figure 6 shows the result. Here local HI surface density at a particular radius is plotted against local surface brightness at that radius. Early-type galaxies (Sa–Sbc) from the Wevers et al. sample have been omitted, in order to avoid comparing very different types of galaxies.

Many of the galaxies show a central depression, but it is clear that outside these central dips the surface density-surface brightness relations for the different galaxies looks similar.

Note that U6614 (the dashed line in the lower-left of the figure) turns out to be the odd galaxy in the LSB samples. It has high surface brightnesses in the inner parts and low HI surface densities, showing that these Malin-1-cousins belong to a different class of LSB galaxies. The early-type galaxies from the Wevers sample, that have been omitted from this plot, also show similar profiles.

Figure 6 shows that the normal LSB galaxies follow a relationship between σ_{HI} and μ_B that is similar to that of late-type HSB galaxies (albeit starting at a lower σ_{HI}), suggesting that LSB galaxies as a whole may be similar to the outer parts of late-type HSB galaxies, and that *local* baryonic surface density controls the current evolutionary rate.

However, one should keep in mind that at identical *local* surface brightnesses LSB galaxies are in general bluer (de Jong 1995) and have lower abundances (McGaugh 1994) than HSB galaxies. This is most likely an effect of the different evolutionary history of LSB galaxies. Summarizing, *local* surface density controls the current evolutionary rate, i.e. the rate at which processes happen at this moment, while the *global* properties show us the total amount of evolution that a galaxy has undergone over its lifetime. The change in global properties is therefore ultimately governed by *local* processes.

8 ROTATION CURVES

In order to intercompare the rotation curves in Fig. 2 we present them again in Fig. 7. The rotation velocity is given as a function of linear distance from the centre. Velocities and linear distances along the major axis have been computed using the inclinations and distances given in Tables 2 and 3. It is clear that most of the rotation curves have maximum rotation velocities between 50 and 120 km s⁻¹. Some of the LSB galaxies are among the slowest rotators known (~ 30 km s⁻¹). Only a few of the rotation curves show clear signs of flattening off. Usually the velocity is still increasing at the outermost measured point.

In order to compare the rotation curves of LSB galaxies with those of other galaxies we have retrieved a number of well-determined rotation curves of HSB galaxies from the literature (see Broeils 1992 and references therein and Table A3).

The rotation curves are shown in Fig. 8, together with the rotation curves from Broeils. In order to compare only galaxies that are morphologically similar to LSB galaxies we have plotted only HSB galaxies with Hubble-types Sc or later. Also plotted are rotation curves of the sample of LSB galaxies from vdH93. The sample of vdH93 generally contains on average more massive LSB galaxies, as can be seen in Fig. 8.

It is clear from Fig. 8 that the rotation curves of LSB galaxies look similar to those of late-type “normal” galaxies, when expressed in scale lengths. We use the scale length of the optical disc as this is the only easily observable length scale in a galaxy, which is intrinsic to the galaxy, in sharp contrast with more arbitrary length scales like isophotal radii or linear radii (see Section 7.1.1). The scale lengths of LSB galaxies are approximately twice as large as those of HSB galaxies at a fixed maximum rotation velocity (ZHBM), so when expressed in kpc, the rotation curves will rise more slowly to their maximum velocity than those of HSB galaxies.

We want to stress here that our rotation curves of LSB galaxies are measured out to a comparable number of scale lengths as the average rotation curve of a HSB galaxy (cf. Fig. 8). Differences between the rotation curves can therefore not be caused by sampling of different length scales due to the larger scale lengths of LSB galaxies.

The larger values for scale lengths of LSB galaxies are shown in Fig. 9, where the scale lengths in the HSB and LSB samples are shown versus their corresponding maximum rotation velocities. The points that represent the LSB galaxies in general are located at larger scale lengths than

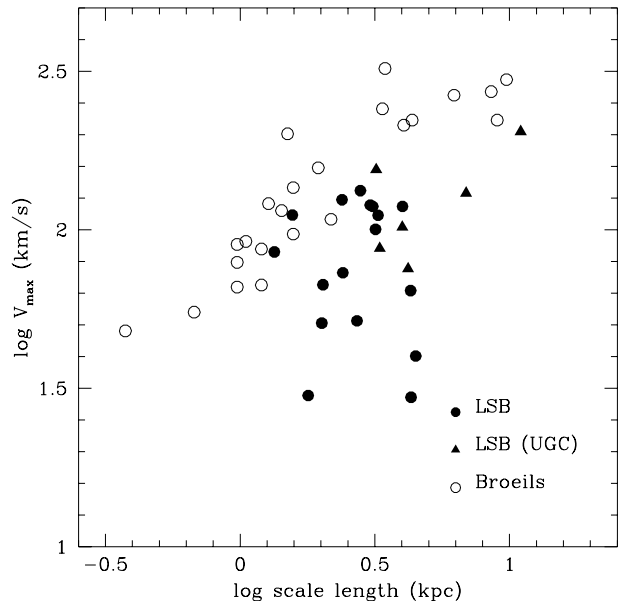


Figure 9. Maximum rotation velocities plotted versus scale lengths. Open symbols are all galaxies from Broeils (1992); filled circles are LSB galaxies from our sample; filled triangles are LSB galaxies from vdH93. It is clear that LSB galaxies have larger scale lengths at a fixed maximum rotation velocity.

those of HSB galaxies at the same velocity. It is striking that the LSB galaxies only occupy the part of the figure with $V_{\max} < 200$ km s⁻¹. Our sample therefore does not contain the equivalents of the large HSB galaxies, that have been so well studied in H_I. We must probably find these large LSB galaxies among the likes of UGC 6614: the Malin-1 cousins (Sprayberry et al. 1995a).

8.1 Compactness

The outer parts of rotation curves are usually assumed to be determined by the dark matter halos that surround galaxies (see van Albada and Sancisi 1986). The fact that LSB rotation curves rise more slowly than those of HSB galaxies with the same V_{\max} implies that not only the light but also the matter in LSB galaxies is distributed more diffusely. A naive extrapolation would then suggest that this might also apply to the dark matter, but an answer to this question will have to wait for full disc-halo decompositions of the rotation curves, which we will discuss more extensively in a forthcoming paper (de Blok & McGaugh, 1996a).

If the differences in surface density are the fundamental criterion that distinguishes HSB galaxies from LSB galaxies, one would like to have a quantitative measure for it. We will therefore use the compactness or the value of the characteristic mass surface density $\sigma \propto V_{\max}^2/h$, where h is the exponential scale length expressed in linear units. It is easy to see that combining the equations $M \propto V^2h$ and $M \propto \sigma h^2$ leads to the above result. Here M is the dynamical mass within a fixed number of scale lengths.

We will now compare the compactnesses with the slopes of the rotation curves. Casertano and van Gorkom (1991), Persic & Salluci (1991) and Broeils (1992) already pointed

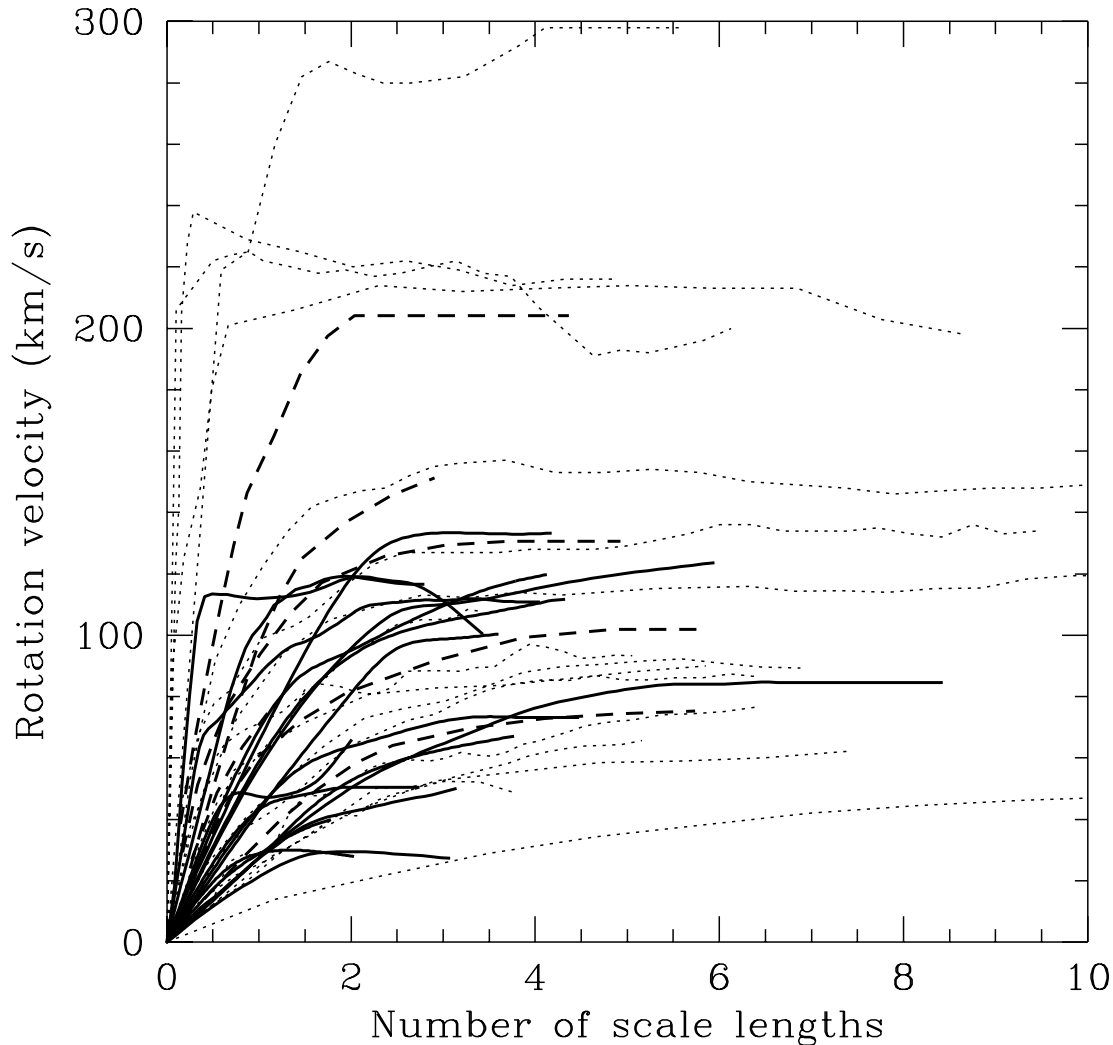


Figure 8. Rotation curves of LSB galaxies from our sample (full lines), LSB galaxies from vdH93 (dashed lines) and HSB galaxies from Broeils (1992) (dotted lines), plotted versus the number of scale lengths.

out that there is a relation between the outer slope of the rotation curve and the maximum rotation velocity. Low-luminosity dwarfs rotate slowly, and have rising rotation curves at the edge of the observed HI disc. Compact high-luminosity galaxies (with high rotation velocities) have declining rotation curves. As compactness in our definition depends on the maximum rotation velocity this implies a relation between the compactness of a galaxy and the slope of its rotation curve.

Following Casertano and van Gorkom (1991) and Broeils (1992) we define the slope as the slope of a straight-line fit to the logarithmic rotation curve (i.e., $d \log V / d \log R$, as this ratio is distance-independent), between an inner ra-

dius, defined as two-thirds of the optical radius R_{25} , and the last measured point of the rotation curve. The decreasing R_{25} towards later types and LSB galaxies does not affect the value of the slope much.

Figure 10 shows the comparison of compactness and slope for HSB and LSB galaxies. The rotation curves of the LSB galaxies have positive slopes in the outer parts, but not more positive than those of classical HSB galaxies. In fact the only thing that distinguishes the LSB galaxies from the HSB galaxies is that their “compactness” or mass surface density is significantly lower than that of HSB galaxies with comparable slope. It is important to note that this surface density includes all mass, light and dark matter.

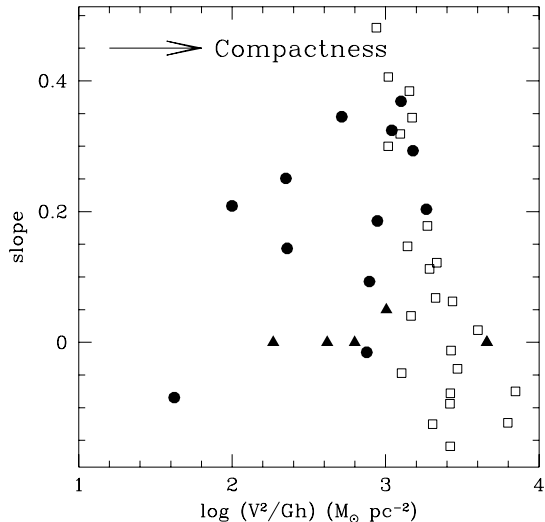


Figure 10. The compactness or mass surface density of HSB and LSB galaxies. It is clear that although some LSB galaxies have comparable compactness as HSB galaxies, some have compactnesses that are a factor of ~ 10 smaller. The open squares denote the galaxies from Broeils (1992), while the filled circles represent the LSB galaxies from this work. Filled triangles are LSB galaxies from vdH93.

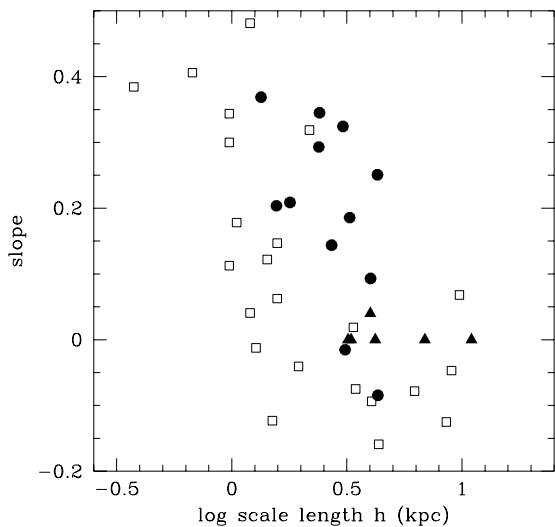


Figure 11. The distribution of logarithmic slope $d \log V / d \log R$ of the rotation curves of HSB and LSB galaxies with scale length. The open dots denote the galaxies from Broeils (1992), while the filled circles represent the LSB galaxies from this work. Filled triangles are LSB galaxies from vdH93.

We can also see that the trend Broeils (1992) has found of slope with scale length has disappeared for scale lengths smaller than 5 kpc (see Fig. 11). At scale lengths smaller than 5 kpc the whole range of slopes is covered. At scale lengths larger than 5 kpc there seem to be virtually no galaxies with positive slopes. Most of the galaxies plotted there are galaxies of types Sc and earlier. However, the presence of giant LSB galaxies at scale lengths between 8 and 10 kpc suggests that the area between 5 and 8 kpc is only empty because of selection effects. Galaxies with identical scale lengths can have rotation curves with different slopes. There does, however, seem to be a tendency for smaller galaxies to show a larger range of (mostly positive) slopes than the larger galaxies.

The rotation velocity, the shape of the rotation curve, the mass surface density and the surface brightness are therefore all related to the compactness of a galaxy. This strongly suggests that the mass is not the only parameter that determines the evolution of a galaxy. *The “compactness” of a galaxy is also an important parameter for the evolution of a galaxy.*

9 MASS TO LIGHT RATIOS

9.1 Relation of M_{HI}/L with central surface brightness

A tracer for the state of evolution of galaxies is the amount of HI gas that is present with respect to the amount of light: M_{HI}/L_B . In order to get a good picture of how this ratio changes with e.g. luminosity or surface brightness one needs a sample of undisturbed spirals of as large a range in central surface brightness and luminosity as possible. The sample of de Jong (1995) is a good sample for this purpose.

We have taken the luminosities and HI masses of this sample of 86 face-on spiral galaxies with accurate photometry and spanning a large range of surface brightness, and calculated the M_{HI}/L_B of the galaxies in the sample. The HI data was taken from the literature (RC3).

The top panel in Fig. 12 shows the HI masses of the galaxies in the sample plotted against their B -band luminosities. It is clear that LSB galaxies have more HI at a fixed luminosity than HSB galaxies. To show that this effect is real and not e.g. caused by colour effects (as LSB galaxies are bluer), we have re-plotted the data in the bottom panel of Fig. 12, this time using the I -magnitudes. This shows that over a large range in luminosity LSB galaxies contain more atomic gas per solar luminosity than their HSB counterparts. This may indicate that either LSB galaxies are really gas-rich (i.e. have a high gas-fraction $M_{\text{gas}}/M_{\text{stars}}$), or that the importance of the (non-observed) molecular gas increases towards higher surface brightnesses (so that $M_{\text{gas}}/M_{\text{stars}}$ might still have similar values for all surface brightnesses). However, in order to explain the trend assuming the latter possibility, there needs to be ~ 10 times more molecular gas than atomic gas in the highest surface brightness galaxies (assuming that LSB galaxies have negligible amounts of molecular gas, which seems to be supported by observations[§]). These large amounts are not consistent with

[§] Recently Wilson (1995) has measured CO/H₂ conversion fac-

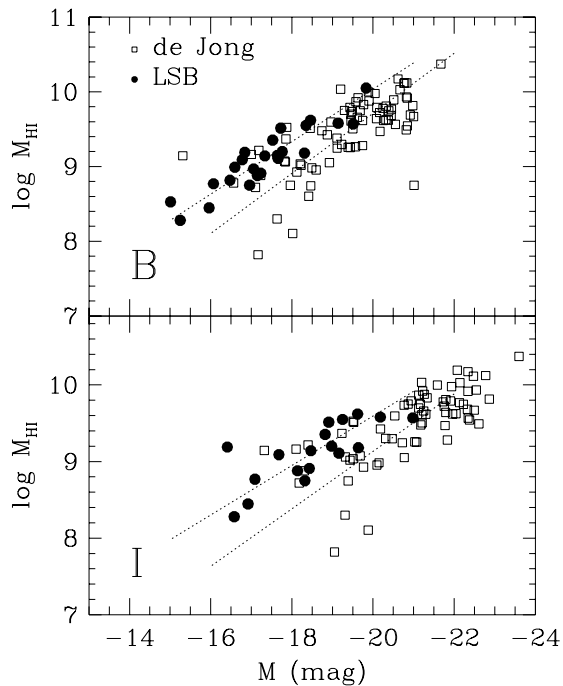


Figure 12. The HI masses of the galaxies in the sample of de Jong and our sample plotted versus their luminosities. The top panel contains *B*-band data. The bottom panel *I*-band data. The two lines are double least-square fits made to both samples separately. There is some overlap between the two samples as de Jong’s sample also contains a number of LSB galaxies. At a fixed luminosity LSB galaxies contain about 3 times more HI.

determinations of molecular gas masses in early-type HSB galaxies (Young & Knezek 1989).

The ratio M_{HI}/L is therefore larger for LSB galaxies, but as Fig. 6 shows, both HSB and LSB galaxies have the same ratio σ_{HI}/μ_B . As LSB galaxies do form (and have formed) fewer stars than HSB galaxies, but have higher gas fractions, the conclusion must be that LSB galaxies have lower HI surface densities. This means that the HI disks *must* be more extended in order to still reach their measured total HI masses, which are quite similar to those of HSB galaxies. Clear differences therefore exist in galaxies of different surface brightness.

9.2 Relation of M_{dyn}/L with central surface brightness

Gas and stars form only the visible part of galaxies. In order to find possible relations of surface brightness with the total mass of galaxies one needs to investigate the behavior of M_{dyn}/L_B . Here we will only discuss this parameter in a

tors as a function of metallicity Z . At $Z = 0.1Z_{\odot}$ – a typical value for the abundances in LSB galaxies – the factor increased by a factor of ~ 5 , with respect to the Galactic conversion factor. This is not enough to allow for much H_2 in LSB galaxies, based on the upper limits measured by Schombert et al. (1990) and de Blok (in prep.).

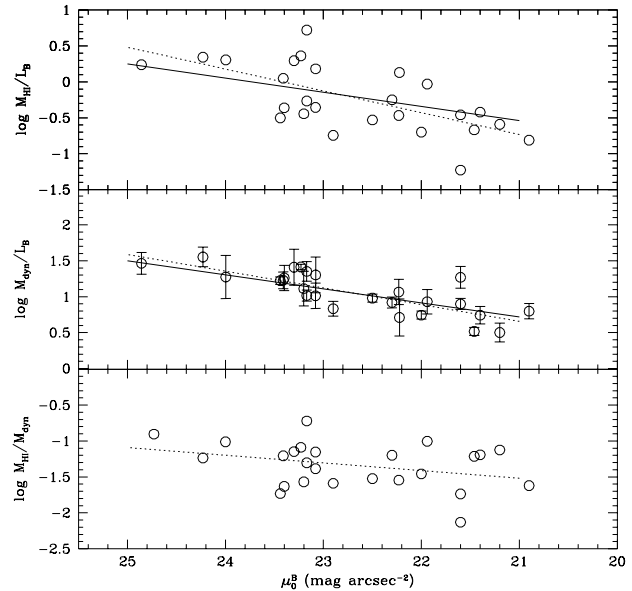


Figure 13. Various mass-to-light ratios for a sample of spiral galaxies of different surface brightnesses. The sample of Broeils (1992) was used, together with LSB galaxies from this work with well-determined inclinations. See Table A3 for identifications. The top panel shows the ratio of hydrogen mass to luminosity. The full line the theoretical expectation from the $\Upsilon\Sigma$ -relation ($\Sigma\Upsilon^2 = \text{constant}$, where $\mu \propto -2.5\log\Sigma$), normalized to go through the data points. The dotted line is the least-squares fit to the data. The middle panel shows the ratio of total mass within $4h$ to luminosity. The full line is again the $\Upsilon\Sigma$ -relation, and the dotted line a least-squares fit to the data. The bottom panel shows the ratio of hydrogen mass and total mass within $4h$. The dotted line is a least-squares fit to the data points.

very global way. An extensive discussion of M_{dyn}/L_B , using disc-halo decompositions of the rotation curves will be the subject of a separate paper. We will merely note that a strong relation of M_{dyn}/L_B with surface brightness exists. This is shown in the middle panel of Fig. 13 where the mass to light ratio M_{dyn}/L_B is plotted as a function of central surface brightness. The HSB galaxies are from the sample of Broeils (1992), the LSB galaxies are from our sample. We have adopted four scale lengths as a consistent definition (MB94, BHB95, ZHBM) of the optical radius, where we determine both the mass and the light. This then is the M/L within the adopted “optical radius” $R_{\text{opt}} = 4h$. We of course cannot measure the *total* mass, just that enclosed by the light. Note that these mass measurements are sensitive to the inclination corrections. It is thus important that the inclination be accurately measured, and we have retained only galaxies which have adequate inclination determinations. Errorbars in Fig. 13 are based on a pessimistic error estimate of 6 degrees. See Table A3 for the identifications of the galaxies plotted.

The derived mass is also sensitive to the measured value of the asymptotic velocity itself, so we have used only those galaxies for which this can be taken directly from a full rotation curve. A strong correlation is apparent: this is the mass-to-light-ratio (Υ) – surface brightness (Σ) relation

from ZHBM. At the highest surface brightnesses, the mass to light ratio is similar to that expected from stellar population models. At the faintest surface brightnesses, it has increased by a factor of ten, indicating increasing dark matter domination within the optical disc as surface brightness decreases, maybe in combination with a systematic change in the stellar population. The slope of the full line in Fig. 13 was forced to equal the value required by the $\Upsilon\Sigma$ -relation and has been shifted to go through the data points. The dotted line is the actual least-squares fit to the data points. These two fits are identical within the errors.

9.3 Hydrogen and total masses

In the top panel of Fig. 13 we have plotted M_{HI}/L_B for the same galaxies as a function of central surface brightness. It is striking that this bears a strong resemblance to the $\Upsilon\Sigma$ -relation. The full line shown in the top panel of Fig. 13 is the $\Upsilon\Sigma$ -relation. The dotted line is again the actual least-squares fit to the data. The $\Upsilon\Sigma$ -relation, which is a relation between dynamical mass and surface brightness, is therefore also a good description for the relation between gas mass and surface brightness.

The relation shown in the top panel of Fig. 13 is independent of the dynamics of the galaxies, while the $\Upsilon\Sigma$ -relation is not. This strong relation of M_{HI}/L_B strongly suggests an evolutionary solution to the $\Upsilon\Sigma$ -relation, as argued by ZHBM. This could, for example, be in the form of HI as a tracer of dark matter (Bosma 1981), or in the form of dark matter as cold gas (Pfenniger et al 1994). A possible problem for an evolutionary solution, however, is that the large values for M_{dyn}/L derived for LSB galaxies imply that the contribution of baryons is not important.

The slight difference between the slopes in the top and middle panels of Fig. 13 introduces a small residual trend of M_{HI}/M_T with surface brightness. This is presented in the bottom panel of Fig. 13. The dotted line is a least-squares fit to the data. This trend may be caused by the increasing importance of atomic gas towards lower surface central surface brightnesses. Rotation curve decompositions are needed to solve this puzzle. However, real variations in M_{HI}/M_T would make evolutionary scenarios less attractive.

We therefore conclude that LSB galaxies are more gas-rich than HSB galaxies, implying that they have systematically higher gas-fractions. This shows again clearly that evolutionary differences exist between galaxies of different surface brightnesses.

10 CONCLUDING REMARKS

In this paper we have presented the HI properties of a sample of 19 late-type LSB galaxies, representative of the LSB galaxies in the SBSM catalogue, determined from observations with the VLA and WSRT.

We have shown that these late-type LSB galaxies have low HI surface densities, both average and local values are about a factor of ~ 3 lower than those in comparable late-type HSB galaxies.

By comparing local surface brightnesses and HI surface densities from galaxies over a large range in surface brightness, we show that both HSB and LSB galaxies follow the

same surface brightness–atomic gas surface density trend. LSB galaxies may in that respect resemble the low surface brightness outer parts of HSB galaxies. Other evidence (e.g. colours and metallicities) suggests that they may be less evolved. Local surface density seems to control the rate of evolution.

Rotation curves rise to maximum velocities between 50 and 120 km s⁻¹, and usually have not flattened off in the outermost point. They rise more slowly towards their asymptotic value than those of comparable HSB galaxies, suggesting an overall lower mass surface density (see also de Blok & McGaugh 1996b): one might speculate that even the dark matter of LSB galaxies may have a lower surface density. A confirmation of this will have to wait for full disc-halo decomposition analysis of the rotation curves (de Blok & McGaugh 1996a).

The late-type LSB galaxies in our sample have higher gas fractions than HSB galaxies, and establish a relation between M_{HI}/L_B and central surface brightness. A similar relation between M_{dyn}/L_B and central surface brightness also exists. This confirms the $\Upsilon\Sigma$ -relation found by ZHBM. All of this may point at an evolutionary solution for the $\Upsilon\Sigma$ -relation, but the high values for M_{dyn}/L argue against this. This remains a major puzzle.

Evolution, compactness, surface density and surface brightness are intimately related. The LSB galaxies we have investigated have low baryonic surface densities and are in all probability slowly evolving systems.

ACKNOWLEDGMENTS

We thank Adrick Broeils for making some of his tables available in electronic form and Adwin Boogert for doing the observations at the Dutch Telescope at La Silla. We also like to thank Renzo Sancisi and Rob Swaters for many useful discussions and constructive suggestions. dB would like to thank the Leidsch Kerkhoven-Bosscha Fonds for travel grants during the writing of this paper. We thank Jon Davies for his comments on an earlier version of this paper.

REFERENCES

- Allen, R.J., Shu, F.H., 1979, ApJ, 227, 67
- Begeman K.G., 1987, PhD thesis, University of Groningen
- Begeman K.G., 1989, A&A, 223, 47
- Bergvall N., Rönnback J., 1994, A&AS, 108, 193
- Bos A., Raimond E., van Someren Greve H.W., 1981, A&A 98, 251
- Bosma A., 1981, AJ, 86, 1825
- Bothun, G.D., Schombert, J.M., Impey, C.D., Sprayberry, D., McGaugh, S.S., 1993, AJ, 106, 530
- Broeils A.H., 1992, PhD thesis, University of Groningen
- Carignan C., 1985, ApJSup, 58, 107
- Carignan C., Beaulieu, S., 1989, ApJ, 347, 760
- Carignan C., Freeman, K.C., 1988, ApJLett, 332, L33
- Carignan C., Puche, D., 1990, AJ, 100, 641
- Carignan C., Sancisi R., van Albada T.S., 1988, AJ, 95, 37
- Casertano S., van Gorkom J.H., 1991, AJ, 101, 1231
- Cayatte V., Kotanyi C., Balkowski C., van Gorkom J. H., 1994, AJ, 107, 1003
- Côté S., Carignan C., Sancisi R., 1991, AJ, 102, 904
- Dalcanton J.J., Spergel D.N., Summers F.J., 1995, preprint

- Davies, J. I., Disney, M. J., Phillips, S., Boyle, B. J., Xouch, W. J., 1994, MNRAS, 269, 349
- Davies, J. I., Phillips, S., Disney, M. J., 1988, MNRAS, 231, 69p
- de Blok W.J.G., McGaugh, S.S., 1996a, in preparation
- de Blok W.J.G., McGaugh, S.S., 1996b, ApJL, in press
- de Blok W.J.G., van der Hulst J.M., Bothun G.D., 1995, MNRAS, 274, 235 (BHB95)
- de Jong R.S., 1995, PhD thesis, University of Groningen
- de Jong R.S., 1996, A&A, in press
- de Vaucouleurs A., de Vaucouleurs G., Buta R.J., Corwin Jr. H.G., Fouqué P., Patreul G., 1991, Third Reference Catalogue of Bright Galaxies (RC3), Springer-Verlag, New York
- Flores, R. A., Primack, J. R., 1994, ApJ, 412, 443
- Freeman K.C., 1970, ApJ, 160, 811
- Guiderdoni, B., Rocca-Volmerange, B., 1987, A&A, 186, 1
- Hodge, P.W., 1967, ApJ, 148, 719
- Hoffman, G.L., Salpeter, E.E., Farhat, B., Roos, T.G., Williams, H.L., Helou, G., 1996, ApJS, in press
- Impey, C., Bothun, G., 1989, ApJ, 341, 89
- Irwin, M. J., Davies, J. I., Disney, M. J.; Phillipps, S., 1990, MNRAS, 245, 289
- Jobin M., Carignan C., 1990, AJ, 100, 648
- Kent S.M., 1986, AJ, 91, 1301
- Kent S.M., 1987, AJ, 93, 816
- Landolt A.U., 1992, AJ, 104, 340
- Maloney P., 1993, ApJ, 414, 41
- McGaugh S.S., 1994, ApJ, 426, 135
- McGaugh S.S., 1996, MNRAS, in press
- McGaugh S.S., Bothun G.D., Schombert J.M., 1995, AJ, 110 573
- McGaugh S.S., Schombert J.M., Bothun G.D., 1995, AJ, 109, 2019
- McGaugh S.S., Bothun G.D., 1994, AJ, 107, 530 (MB94)
- Mo, H. J., McGaugh, S.S., Bothun, G. D., 1994, MNRAS, 267, 129
- Persic M., Salucci P., 1991, ApJ, 368, 60
- Pfenniger D., Combes F., Martinet L., 1994, A&A, 285, 79
- Puche D., Carignan C., Bosma A., 1990, AJ, 100, 1468
- Puche D., Carignan C., Wainscoat R.J., 1991, AJ, 101, 447
- Quinn, T., Katz, N., Efstathiou, G., 1995, preprint
- Roberts M.S., Haynes M.P., 1994, A&AR, 32, 115
- Roelfsema P.R., Allen R.J., 1985, A&A, 146, 213
- Romanishin, W., Krumm, N., Salpeter, E., Knapp, G., Strom, K. M., Strom, S. E., 1982, ApJ, 263, 94
- Rönnback J., 1993, PhD thesis, University of Uppsala
- Rönnback J., Bergvall N., 1995, preprint
- Schombert J.M., Bothun G.D., Impey C.D., Mundy L.G., 1990, AJ, 100,1523
- Schombert J.M., Bothun G.D., 1988, AJ, 95, 1389
- Schombert J.M., Bothun G.D., Schneider S.E., McGaugh S.S., 1992, AJ, 103, 1107 (SBSM)
- Schwartzberg J.M., Phillips S., Smith R.M., Couch W.J., Boyle B.J., 1995, MNRAS, 275, 121
- Sprayberry D., Bernstein G.M., Impey C.D., Bothun G.D., 1995, ApJ, 438, 72
- Sprayberry D., Impey C.D., Bothun G.D., Irwin M., 1995, AJ, 109, 558
- Turner, J. A., Phillipps, S., Davies, J. I., Disney, M. J., MNRAS, 1993, 261, 39
- van Albada T.S, Sancisi R., 1986, Phil. Trans. R. Soc. Lond. A, 320, 447
- van der Hulst J.M., Skillman E.D., Smith T.R., Bothun G.D., McGaugh S.S., de Blok W.J.G., 1993, AJ, 106, 548 (vdH93)
- van der Hulst J.M., Terlouw J.P., Begeman K.G., Zwitser W., Roelfsema P.R., 1992, in Worall D.M., Biemesderfer C., Barnes J., ed., ASP Conf Series Vol. 25, Astronomical Data Analysis Software and Systems I, San Francisco, p. 131
- Warmels R.H., 1988, A&AS, 73, 453
- Wevers B. M. H. R., van der Kruit P. C., Allen R.J., 1986, A&AS, 66, 505
- Wilson C.D., 1995, preprint
- Young J.S., Knezek P.M., 1989, ApJ 347, L55
- Zwaan M.A., van der Hulst J.M., de Blok W.J.G., McGaugh S.S., 1995, MNRAS, 273, L35 (ZHBM)

APPENDIX A: ADDITIONAL OPTICAL OBSERVATIONS

A1 Observations and reduction

A1.1 Jacobus Kapteyn Telescope

CCD imaging for a couple of galaxies in our sample, for which previously no optical information was available (F571-8, F571-V2, F574-1, F579-V1, F583-1 and F583-4), was obtained at the 1 meter Jacobus Kapteyn Telescope[¶] at La Palma, during two nights in March 1995.

Conditions were variable, with an average seeing of 2 to 3 arcsec. *R*-band imaging was obtained using the 1124² TEK chip at the JKT, which was binned to 562² due to the poor seeing conditions. The pixel size therefore became 0.662 arcsec. Images were reduced using standard procedures with the IRAF reduction package. See Table A1 for specific details on the observations. See BHB95 for a complete description of the reduction procedures.

The images were flux-calibrated using standard stars from the list of Landolt (1992). Due to the variable conditions the photometric solution, based on 15 standard star exposures, is formally only accurate to 0.2 magnitudes, but as will be shown later, is likely to be much better than this.

Many images showed a gradient across the sky background. This gradient was removed during the process of sky subtraction, but deviations from the mean sky background resulting from this gradient were later used to estimate uncertainties in the surface brightness of the galaxies. This procedure is also described in BHB95.

A1.2 ESO Dutch Telescope

BRI CCD imaging of F583-1 was obtained at the 90 cm Dutch Telescope at ESO, Chile, during the night of April 14-15 1994. Conditions were photometric, with an average seeing of 1 arcsec. Imaging was obtained using a 512² TEK chip, with a pixel size of 0.457 arcsec. Images were reduced using standard procedures (see above). Calibration was performed using Landolt (1992) standard stars. Photometric solutions had an accuracy of 0.03 mag in *B*, *R* and *I*. See Table A1 for a journal of the observations.

A2 Radial profiles

A2.1 Derivation

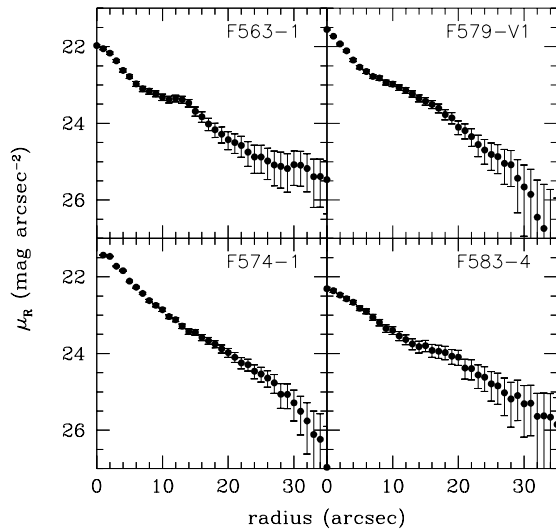
For each galaxy ellipse fit were made to the outer isophotes, and radial profiles were produced using the inclinations and

[¶] The Jacobus Kapteyn Telescope is operated by the Royal Greenwich Observatory at the Observatorio del Roque de los Muchachos of the Instituto de Astrofísica de Canarias with financial support from the PPARC (UK) and NWO (NL).

Table A1. Journal of observations

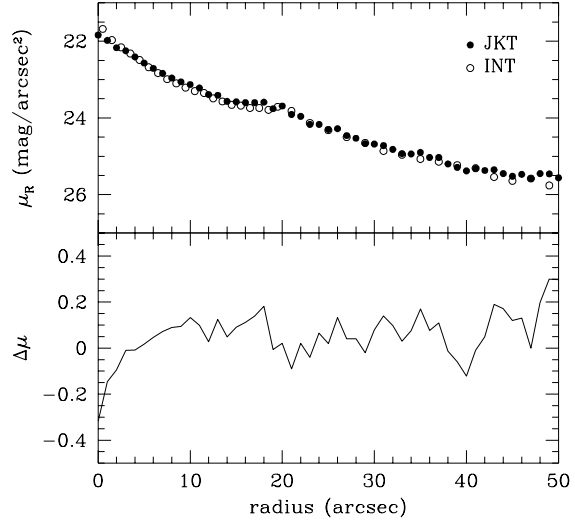
Name (1)	date (2)	filter (3)	exposure (4)
La Palma			
F563-1	Mar 7 '95	R	4×900
	Mar 8	R	2×900
F571-8	Mar 2	R	4×900, 600
F571-V2	Mar 2	R	2×900, 600
F574-1	Mar 2	R	4×900
F579-V1	Mar 2	R	3×900
F583-1	Mar 7	R	3×900
F583-4	Mar 8	R	2×900
La Silla			
F583-1	Apr 14 '94	B	9×300
		R	7×300
		I	6×300

- (1) Name of the galaxy
(2) Date at the beginning of the night
(3) Photometric band
(4) Exposure time in seconds of individual observations

**Figure A1.** Radial R -band profile of F563-1, F574-1, F579-V1 and F583-4.

position angles thus derived. The central surface brightness and scale length of the disc were derived by using a decomposition of the profile in an exponential disc and an exponential bulge. In practice the contribution of the bulge was for most of the galaxies negligible.

The optical structural parameters thus derived are given in Table A2, along with the total magnitudes and isophotal radii. Note that the central surface brightnesses are the measured values: no correction has yet been made for inclination and Galactic foreground extinction. Figure A1 presents the radial R -band profiles of F563-1, F574-1, F579-V1 and F583-4.

**Figure A2.** Comparison of the radial profiles of F563-1, using the new data presented here (closed dots) and the data from BHB95 (open dots). To produce the profiles the ellipse parameters from BHB95 have been used.

A2.2 Note on F563-1: Comparison with other data

Comparison with BHB95 will show that the optical inclination of F563-1 given here is substantially different from their inclination. This is because the image in BHB95 suffered from a modest amount of stray light and it was therefore not clear whether the extended face-on like structure around F563-1 was real or not. The images obtained at the JKT show that indeed this galaxy is surrounded by a faint face-on-like disc. The old inclination in BHB95 was determined using the inner barlike structure, yielding a value of 50 degrees. The new value of 25 degrees derived here, is in much closer agreement with the HI data.

We have determined the radial profile of F563-1 from the new JKT imaging data, using the inclination and position angle given in BHB95. This is shown in Fig. A2, where we have also plotted their INT profile of F563-1. The two profiles are clearly indistinguishable. Only at very low surface brightnesses does the JKT profile diverge from the INT profile. This is simply because the JKT imaging has a lower signal to noise ratio than the INT imaging of BHB95. This suggests that the surface brightnesses presented here are likely to be more accurate than the uncertainty of 0.2 magnitudes which is given by the formal photometric fit to the standard stars.

A2.3 Notes on F571-8: an edge-on LSB galaxy

This galaxy is the only edge-on galaxy in our sample. During the initial sample selection the faint edge-on disc was not noticed, and only showed up in the HI and subsequent optical observations. As the usual ellipse fitting methods and integrating in rings to produce the radial profile, do not work for edge-on galaxies, we have produced the radial

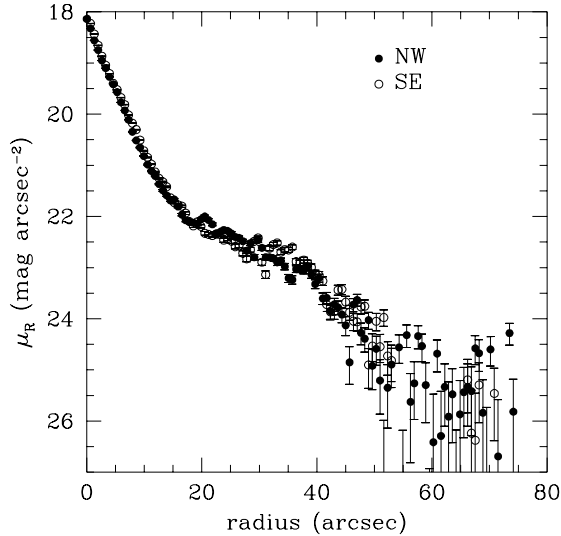


Figure A3. Major axis R -band profile of F571-8. The profile has a width perpendicular to the major axis of 1.5 arcsec. The closed circles denote the major-axis light distribution of the NW side of the galaxy, the open circles that of the SE side.

profile as follows. A major axis cut of 2 arcsec width (corresponding to one seeing FWHM) was made, and this profile was subsequently decomposed into a bulge and disc component. This profile is shown in Fig. A3, where the profile is folded around the central position. An exponential bulge was fit to the inner brightness peak, subtracted, and another exponential disc was fit to the residual profile. Structural parameters of these components can be found in Table A2. This galaxy is also special in the sense that it has a very significant bulge, in contrast with all other galaxies in the sample. The magnitudes of the bulge and disc components, and the total galaxy, were measured directly from the optical image by integrating the total fluxes of the components. The structural parameters were therefore not used in determining these quantities. Using these magnitudes yields a bulge-to-disc ratio for F571-8 of ~ 2 , which is much larger than those of the other galaxies in the sample where usually $B/D \ll 0.1$.

The image shows no visible evidence for dust: there is no sign of an equatorial dust lane. This is confirmed by the minor axis profiles: the light distribution above and below the plane is identical for all radii. If F571-8 were representative for the face-on LSB galaxies in this sample, this would confirm the low dust contents for LSB galaxies inferred from colours, observed Balmer decrements and CO fluxes. However, the large bulge of this galaxy probably means that this galaxy belongs in a different class of LSB galaxies. A more extensive study of edge-on LSB galaxies should shed some more light on this.

A2.4 Notes on F583-1: Comparison and colours

Using the procedures described in BHB95 we have determined the radial luminosity and colour profiles of F583-1.

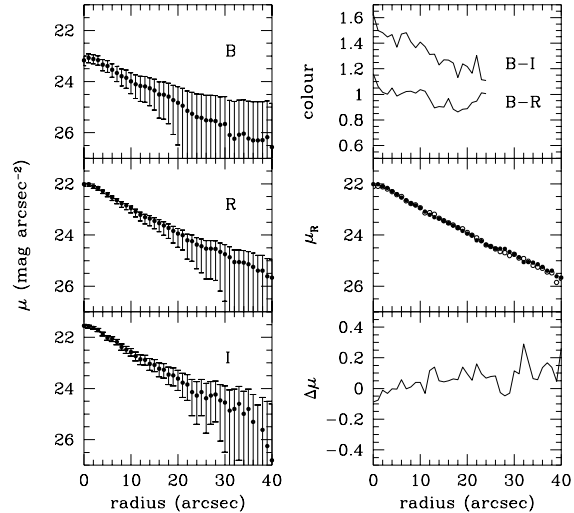


Figure A4. Radial profiles of F583-1. Left row shows, from top to bottom, the measured radial luminosity profiles in the B , R and I bands respectively. The right row shows in the top panel the $B - I$ and $B - R$ radial colour profiles; the middle panel shows a comparison between the R band profiles as obtained with the JKT (open circles) and the Dutch Telescope (filled circles); the bottom panel shows the difference between these two profiles $\Delta\mu = \mu_{Dutch} - \mu_{JKT}$.

These are presented in Fig. A4. The leftmost panels show the radial profiles in B , R and I . The errors represent the maximum errors caused by uncertainty in the value of the sky background. Even though this uncertainty was 3 counts typically, the effects on the values of the surface brightness can be quite severe. Values for surface brightness and scale length are given in Table A2. Comparison with other galaxies from BHB95 shows that this galaxy is a typical LSB galaxy in all respects. The colours (shown in top-right panel of Fig. A4) are also quite normal for LSB galaxies. We find that in F583-1 the average (area weighted) value for $B - R$ is 0.95, which is slightly redder than the typical value of the sample of BHB95, but still well within the range covered by LSB galaxies. The area weighted value for $B - I$ is 1.35, which is almost the typical value found for the sample of BHB95.

The two panels at bottom-right compare the present data with data obtained with the JKT telescope (see Section A1.1). It is clear that despite the variable conditions during the JKT run, the quantities derived from that data are usually accurate to within a tenth of a magnitude.

A3 Conversion to B -band

In order to make this data directly comparable with the data from BHB95, used in this paper to discuss the properties of LSB galaxies, we have converted the R surface brightnesses and magnitudes of F571-8, F574-1, F579-V1 and F583-4 to the B -band using the median colours of the sample of LSB galaxies discussed in BHB95.

As the median $B - R$ colour of LSB galaxies is +0.78, we have assumed that $\mu_B(0) = \mu_R(0) + 0.78$. This value for $\mu_B(0)$ was furthermore corrected for inclination, and these are then the values given in Table 3.

As is shown in BHB95, there is also a small change in scale length between B and R -band. However this change is much smaller than the uncertainty introduced by the correction of the surface brightness, and we have therefore assumed that $h_B = h_R$.

Total R -band magnitudes underwent a similar correction: as we have assumed the scale length to be constant, we can compute $m_{T,B} = m_{T,R} + 0.78$. From this one can compute values for L_B and M_B , which are given in Table 3.

The corrections made to the values derived for F571-8 are of a different nature. In converting the edge-on central surface brightness of the disc, as measured from the major axis profile, to a face-on surface brightness, we have assumed the disc to be completely optically thin. This is probably an oversimplification, however, evidence that LSB galaxies may not contain as much dust as normal HSB galaxies, also invalidates using the standard corrections for internal extinction. In the case of zero internal extinction the face-on central surface brightness is simply half that as measured edge-on (0.75 magnitudes fainter). To this face-on value we also added the colour correction of 0.78 magnitudes, yielding the value given in Table 3. The same assumptions were made in determining the luminosity of the disc: optically thin, and a colour correction of 0.78 magnitudes.

A4 Identification of galaxies in Fig. 13

Table A3 contains the identification of the galaxies plotted in Fig. 13. Also given are the sources for the data. We retrieved the surface brightnesses from the original papers (see notes to Table A3 for a complete list), and where necessary converted to the B -band.

Table A3. Identification of galaxies in Fig. 13

Name (1)	Ref (2)	Name (3)	Ref (4)
DDO 154	1,2	NGC 5033	3,9
DDO 168	3	NGC 5585	13
NGC 55	4	NGC 6674	3
NGC 247	5,6	NGC 7331	3,9
NGC 300	7,6	UGC 2259	14,9
NGC 801	3,8	UGC 2885	15,8
NGC 1560	3	F568-3	16,17
NGC 2403	9,10	F568-V1	16,17
NGC 2841	9,10	F571-V1	16,17
NGC 2903	9,10	F563-V2	18,17
NGC 2998	3,8	UGC 128	19
NGC 3109	11,10	UGC 6614	19
NGC 3198	12,10		

Columns:

(1),(3) Name of the galaxy.

(2),(4) Source of the data.

Sources:

- [1] Carignan & Freeman (1985)
- [2] Carignan & Beaulieu (1989)
- [3] Broeils (1992)
- [4] Puche, Carignan & Wainscoat (1991)
- [5] Carignan & Puche (1990)
- [6] Carignan (1985)
- [7] Puche, Carignan & Bosma (1990)
- [8] Kent (1986)
- [9] Begeman (1987)
- [10] Kent (1987)
- [11] Jobin & Carignan (1990)
- [12] Begeman (1989)
- [13] Côté, Carignan & Sancisi (1991)
- [14] Carignan, Sancisi & van Albada (1988)
- [15] Roelfsema & Allen (1985)
- [16] BHB95
- [17] this work
- [18] MB94
- [19] vdH94

Table A2. Parameters of the sample.

Name	filter	i	PA	μ_λ	α	h	m_T	R_{25}	m_{25}	M_T	A_λ	Note
(1)	(2)	(3)	(4)	(5)	(6)	(7)	(8)	(9)	(10)	(11)	(12)	(13)
F563-1	R	25	168	22.55	13.0	2.1	15.1	26	16.3	-17.6	0.04	
F571-8	R	90	167	*	*	*	15.0	33	15.0	-17.8	0.00	<i>a</i>
disc		*	*	20.59	16.0	2.8	16.2	*	*	-16.6	*	<i>b</i>
bulge		*	*	18.13	3.3	0.6	15.4	*	*	-17.4	*	<i>b</i>
F574-1	R	65	92	21.60	9.1	3.2	15.7	38	15.8	-18.6	0.05	
F579-V1	R	26	113	21.90	10.0	3.8	15.0	27	15.9	-19.0	0.04	
F583-1	B	63	175	23.05	10.2	1.2	16.0	21	16.5	-15.9	0.09	
	R	63	175	22.01	9.8	1.1	15.1	32	15.3	-16.8	0.06	
	I	63	175	21.38	9.1	1.1	14.6	33	14.8	-17.1	0.04	
F583-4	R	55	116	22.38	11.3	2.0	15.7	27	16.1	-17.1	0.02	

Columns:

- (1) Name of the galaxy.
- (2) Photometric band.
- (3) Inclination as derived from our data.
- (4) Position angle measured from N through E.
- (5) Uncorrected central surface brightness of disc.
- (6) Scale length a in arcsec.
- (7) Scale length h in kpc, using distance from Table 3.
- (8) Total magnitude of exponential disc.
- (9) Radius in arcsec of 25 R -mag arcsec⁻² ellipse.
- (10) Total magnitude m_{25} within 25 R -mag arcsec⁻² ellipse.
- (11) Absolute magnitude, using column 7 and Table 3.
- (12) Applied extinction correction in R .
- (13) Notes: **a)** Magnitudes are determined from the total image, by integrating the flux. R_{25} has been measured in the major axis cut presented in Fig. A3. **b)** The magnitudes of the bulge and disc components are determined directly from the image. The structural parameters were determined from the major-axis cut.